Visual Abstract

High-quality nodule analysis in spheroidal graphite cast iron using X-ray micro-computed tomography

J. C. Toledo
Departamento de Ingeniería Industrial, Universidad Tecnológica Nacional-Facultad Regional Rafaela, Acuña 49, Rafaela, Santa Fe, Argentina
juantoledojn12@gmail.com, http://orcid.org/0000-0002-6047-035X

F. V. Díaz
Departamento de Ingeniería Electromecánica, Universidad Tecnológica Nacional-Facultad Regional Rafaela-CONICET, Acuña 49, Rafaela, Santa Fe, Argentina
felipe.diaz@frra.utn.edu.ar, https://orcid.org/0000-0003-4998-5536

M.E. Peralta
Departamento de Validación de Equipos y Componentes, Instituto Nacional de Tecnología Industrial-Centro Litoral, Ruta Nacional N°34 km 227.6, Rafaela, Santa Fe, Argentina
meperalta@inti.gob.ar, https://orcid.org/0000-0001-5807-8618

D. O. Fernandino
INTEMA, Universidad Nacional de Mar del Plata-CONICET, Av. Colón 10850, Mar del Plata, B7606BVZ, Argentina
dfernandino@fi.mdp.edu.ar, https://orcid.org/0000-0003-4647-2663

ABSTRACT. This work is a continuation of the studies presented in a recent paper by the authors, where a methodology to obtain different nodule quality categories in spheroidal graphite cast iron, was proposed. In this study, an exhaustive analysis of the highest-quality graphite nodules was performed. The experimental methodology involves X-ray micro-computed tomography analysis and digital image post-processing of the high-quality graphite nodule population. Furthermore, different subpopulations were selected, following a nodular size criterion. The procedure involves the evaluation and comparison of the sphericity and compactness distributions and the distances between neighbouring nodules by using ad-hoc image processing software. The results reveal the complementary nature of the sphericity and compactness parameters, which allow classifying, with great accuracy, different nodular quality categories of spheroidal graphite cast iron. Additionally, new viewpoints about the nodular morphology study and the distribution of quality nodules in the metallic matrix were provided, which could be extended to other heterogeneous materials.

OPEN ACCESS

Citation: Toledo, J.C., Díaz, F.V., Peralta, M.E. Fernandino, D.O., High-quality nodule analysis in spheroidal graphite cast iron using X-ray micro-computed tomography, Frattura ed Integrità Strutturale, 62 (2022) 279-288.

Received: 30.07.2022
Accepted: 21.08.2022
Online first: 30.08.2022
Published: 01.10.2022

KEYWORDS. X-ray micro-tomography; Sphericity; Compactness; Nondestructive analysis; Spheroidal graphite cast iron.

INTRODUCTION

Cast iron (CI) is an iron-carbon-silicon cast alloys used to manufacture different components of machines, structures and devices [1]. CI is continually progressing in terms of microstructure and mechanical properties. The microstructure of CI depends on the chemical composition, cooling rate conditions, and subsequent heat treatments [2]. Properly controlling the carbon and silicon contents and the cooling rate, the graphite crystallizes directly from the melt [3,4]. Then, the mechanical properties will strongly depend on the shape, size and distribution of the graphite particles in the metallic matrix. Lamellar graphite, corresponding to grey cast iron, allows generating a material with good casting and machining capabilities but brittle. Nodular graphite, corresponding to spheroidal graphite cast iron (SGI), improves the ductile behaviour and will give good mechanical strength and excellent fatigue properties. SGI has achieved a strong impact since its first application, and it has been researched and applied for several decades. The SGI microstructure is composed of a distribution of quasi-spheroidal graphite nodules embedded in a metallic matrix, which can be modified to obtain different grades of SGI by performing different heat treatments [5]. It is worth noting that the most relevant properties, such as fatigue strength, toughness, mechanical properties, and fracture are related to the graphite nodules morphology in terms of size, nodularity, and nodular count [6-11]. Regarding the damage micromechanisms, the influence of the graphite nodules morphology on SGI for different loading conditions was also analysed in the literature [7,9,12,13]. In general, it was observed that the damage micromechanisms can change or be different depending on the metallic matrix microstructure and the graphite nodules morphology. For example, it was reported that graphite nodules with low nodularity (poor quality) affect the fatigue crack propagation path and the crack growth mechanisms [7,13]. Accordingly, the correct evaluation of the graphite nodules quality is an important task to understand the mechanical response of an SGI component in service.
In this context, the complete characterization of the graphite nodules needs the evaluation of nodular count, size, shape, neighbouring distances, and spatial distribution. This geometrical characterization can be performed by means of using X-ray micro- computerized tomography (μCT) [14-15]. μCT is a non-destructive 3D scanning technique that allows observing the internal structure of the SGI with a very high spatial resolution in the case of small-thickness samples. This technique is based on measuring X-rays attenuation, which is produced when X-rays pass through the sample evaluated in different angular positions. X-rays attenuation generates a data set that is then processed using a reconstruction algorithm to generate the 3D volume [16,17]. Afterwards, the reconstructed volume is observed from a slice (virtual cross-section) or by representing a 3D view containing the internal features of the complete volume. This technique allows characterizing the spatial distribution of graphite nodules with great precision, quantifying the size, shape and location of each nodule regarding a coordinate system [18]. In addition, this technique allows examining the distribution of nodular size, the clustering tendency, and the sphericity (SG) and compactness (C) parameters for each nodule. The SG parameter, commonly evaluated in SGI analysis [19,20] to estimate nodular quality, is obtained from the surface (Ar) and volume (Vr) of the nodule

$$SG = \pi 0.33\ (6Vr)0.67/Ar \tag{1}$$

On the other hand, the parameter C is obtained by relating Vr to the volume of the sphere that circumscribes the nodule (Vs)

$$C = Vr\ /Vs \tag{2}$$

Although this parameter is not usually used as a nodular quality estimator in SGI, the authors recently evaluated SG and C parameters to establish quality categories for graphite nodules from a SGI sample by μCT [21]. In that work, the C parameter was identified as a very good geometric parameter to adequately classify the graphite nodule quality, even better than SG since, although the SG distributions associated with subpopulations of high and medium compactness are similar, the tomographic images show substantial differences in terms of nodular quality of both subpopulations.
This work proposes to continue the above-mentioned study by evaluating a population of 1910 high-quality graphite nodules using μCT and digital image processing. The present study includes the analysis of different subpopulations, which are defined following a nodular size criterion. For these subpopulations, the distances between neighbouring nodules, the spatial

distribution, the tendency to clustering and the relation between SG and C parameters with the nodular size, are explored aiming at the improvement of the quality category classification in spheroidal graphite cast iron and other materials.

EXPERIMENTAL METHODOLOGY

An ad hoc SGI sample (60-40-18 SGI grade according to the ASTM A395) with 6.4 mm x 5.1 mm x 1.2 mm was used to generate the high-resolution 3D images. Details of the testing material can be found in Díaz et al. (2021) [21].

X-Ray Micro-Tomography

The X-ray μCT was performed employing a Phoenix V |tome| x S 240 tomograph (General Electric). It is known that beam hardening occurs when a tomographic image is generated due to preferential absorption of low-energy X-rays [22,23]. Beam hardening produces non-linearity in the X-ray attenuation when it crosses the thickness of the sample and, in addition, different artefacts in the tomographic image [24,25]. Accordingly, a 0.1 mm Cu filter was used to alleviate the artefacts produced since by filtering the source, low-energy X-rays are removed. Additionally, the reconstruction software performs a digital correction of the artefacts generated.

Parameters setting of the μCT procedure.

Optimization of the quality and resolution of the μCT images was performed from an experimental setting of the contrast resolution (CR), the noise, the spatial resolution, and the dimensional uncertainty. The CR allows distinguishing several structures due to their singularity in the grayscale. The noise, caused by the attenuation coefficient variation between voxels [26,27], is related to the amount of signal received by the detector (a high-intensity signal generates an image with a low noise level and high CR). Considering that the contrast-to-noise ratio (CNR) is measurable and improvable, the CNR was used to evaluate the quality of the tomographic image performed [28]. Additionally, if the spatial resolution in the μCT image is high, smaller and closer structures can be distinguished, whereas the size and location of the graphite nodules in the sample are related to the dimensional uncertainty.

Considering the above-mentioned and after some experimental tests, an increase in the acceleration voltage (set at 80 kV) led to a noise reduction, whereas an increase in the filament current (set at 90 μA) led to an improvement in the CR. Using the Phoenix datos|x 2 CT software [29], 20 measurements in different cross-sections of the tomographic image were carried out to obtain the CNR value, which was 10.45. Moreover, spatial resolution was optimized by combining the smallest voxel size and the best magnification [30]. The spatial resolution was about 7 μm/voxel, with a magnification of 27X. 30 tomographic images of steel wire patterns were used to obtain the dimensional uncertainty, which was about ± 5.8 μm, with a confidence level of 95%. Details of the uncertainty calculation can be found in Díaz et al. (2021) [21].

Processing of the data retrieved from μCT analysis

The equivalent diameter, D (the diameter of a circumscribed sphere in the graphite nodule), SG and C parameters were evaluated from 1910 highest-quality nodules, which belong to a region of interest (ROI) of 2.6 x 2.1 x 0.5 mm. Then, the AQ population was defined according to the D, SG and C parameters. Only graphite nodules with a diameter greater than 25 μm were considered to avoid inclusions or micro-shrinkage defects, which are common in cast materials. That population corresponds to the nodules with SG and C values greater than 65% and 50%, respectively. The parameters used to classify each subpopulation and the corresponding count, are listed in Tab. 1, where G1, G2, and G3 correspond to small, medium, and large nodules, respectively. It is worth noting that these values were obtained from an exhaustive evaluation of the SG and C distributions for 9238 nodules, which is detailed in Díaz et al. (2021) [21].

The count shows that small and medium-sized nodules prevail. Fig. 1 shows three quality nodules extracted from each subpopulation. Note that the nodules have the same SG values and different C values. The digital image processing of the μCT images was carried out using Volume Graphics VGSTUDIO MAX 3.0 (version 3.0, Volume Graphics, Heidelberg, Germany) [31]. This software is widely used in many laboratories and industries due to its excellent performance.

Gap definition

The smallest distance between a nodule and the nearest neighbour, called a "Gap", was determined from the surface of the circumscribed sphere of each nodule, as shown in Fig. 2. Therefore, if the nodules evaluated were spheres, the values should be strictly positive or zero. However, the Gap is negative when the circumscribed spheres share a part of their volume, which is expected for low-quality nodules, and rarely occurs for high-quality nodules. Consequently, the Gap values could

be used as an indirect measure of nodular quality. For example, if the percentage of negative values is small, the quality of the nodules will be high.

Population	Subpopulation	Diameter (μm)	Sphericity (%)	Compactness (%)	Count
AQ	G1	25-40	65-100	50-100	724
	G2	40-60	65-100	50-100	852
	G3	60-80	65-100	50-100	334

Table 1: Parameters associated with each subpopulation.

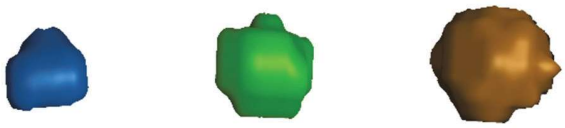

(a) (b) (c)

Figure 1: Nodules from each subpopulation. The parameters are: (a) D = 31 μm, SG = 67%, C = 63%; (b) D = 51 μm, SG = 67%, C = 53% and (c) D = 70 μm, SG = 67%, C = 57%.

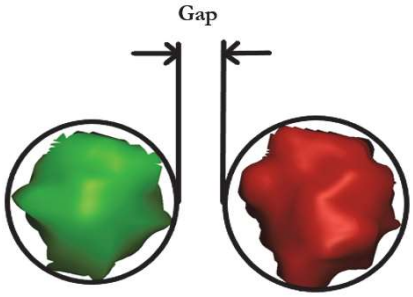

Figure 2: Schematic representation of the Gap parameter.

RESULTS

Spatial distributions and Gap analysis

Fig. 3 shows the spatial distributions of the G1, G2 and G3 subpopulations. This figure corroborates the G1 and G2 high counts and the highest quality of the nodules evaluated. In all cases, the nodules are uniformly distributed. However, in all subpopulations, zones with clustered nodules and zones with nodules following a linear or curved pattern are observed.

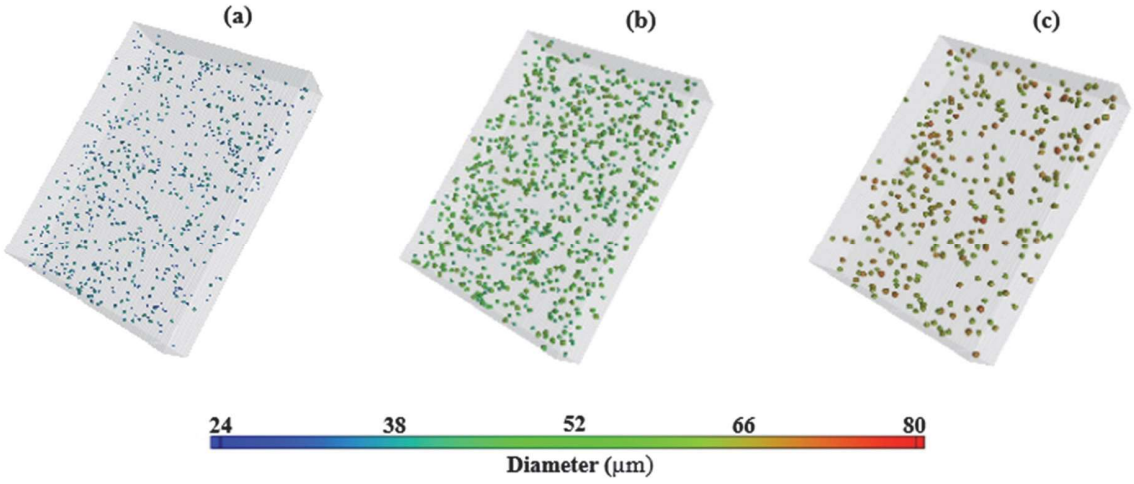

Figure 3: Spatial distribution of nodules in subpopulations: (a) G1, (b) G2 and (c) G3.

Fig. 4 shows the Gap parameter distribution for AQ. Negative values are small (7.4% of the population), indicating the nodular quality is high. Regarding the positive values, the distribution is hyperbolic, with a very high count for the smallest Gap values, which corroborates the clustering tendency of high-quality nodules. Tab. 2 shows the negative Gap nodule count and percentage. This percentage increases when the nodule size increases. The small percentage associated with G1 (small nodules) denotes a high number of high-quality nodules. On the other hand, the percentage is similar for G2 and G3 (medium and large nodules).

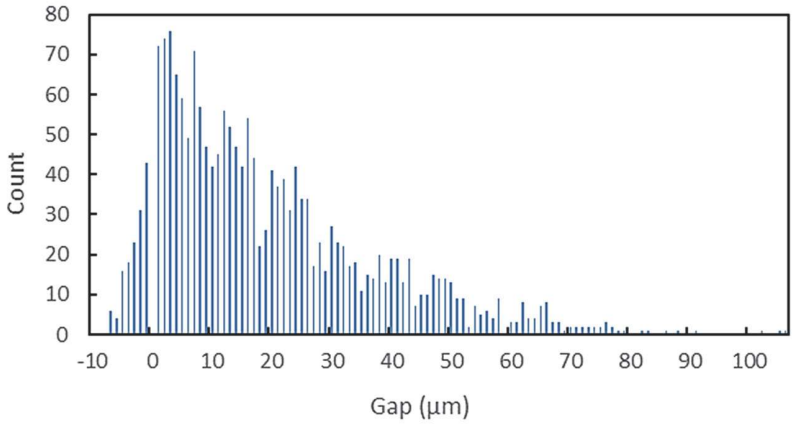

Figure 4: Gap distribution of the AQ population.

Subpopulation	Count	Negative Gap nodule count	Negative Gap nodules (%)
G1	724	18	2.4
G2	852	85	9.9
G3	334	38	11.3

Table 2: Gap values from the evaluated nodules

Sphericity and compactness distribution analysis

The SG and C distributions of the population AQ and its subpopulations G1, G2 and G3 are shown in Fig. 5. The G1 range is wider than the G2 range, which is wider than the G3 range. Therefore, the SG range decreases when the nodule size increases (see Fig. 5a). Fig. 5b shows the C distributions. The ranges of G1, G2 and G3 are similar. The C ranges also decrease when the nodule size increases. Different amplitudes for the ranges of SG and C are observed. For SG, the amplitudes are 14, 10 and 5% for G1, G2 and G3, respectively. For C, the values are 23, 20 and 16% for the same subpopulations. Therefore, the C values are more diverse than the SG values.

In Fig. 5a, AQ initially increases; then, it decreases with a high slope and, finally, it decreases with a low gradient. The shape of AQ in Fig. 5b is similar, but it includes a stationary zone. In both cases, the G2 shape reproduces the AQ shape. On the contrary, the G1 and G3 shapes differ from the AQ shape. In addition, the G2 subpopulation, which contains middling size nodules, shows a significant count and high values of C and SG.

The C distributions of G1 and G2 have similar shapes in the 50-55% range. From 55%, the G2 count is higher than G1 and G3, and the G1 count decreases, approaching the G3 count. For higher values of C, G1 and G3 have similar counts. Furthermore, in the SG range of 65-69%, the G2 count is higher than the G1 count and, in the SG range of 70-75%, the behaviour is the opposite. In the SG range from 65 to 70%, the count is high, and from 71 to 79%, the count is low. Considering the first range (high count), when SG increases, the counts of G1 and G3 increase and decrease, respectively. In the C distribution (range from 50 to 60%), the trend is the opposite because when C increases, the counts of G1 and G3 decrease and increase, respectively.

These results show that small and large nodules have opposite behaviours. Furthermore, these behaviours are reversed when the parameter evaluated changes. Therefore, the SG and C parameters are complementary when small and large nodule subpopulations are evaluated.

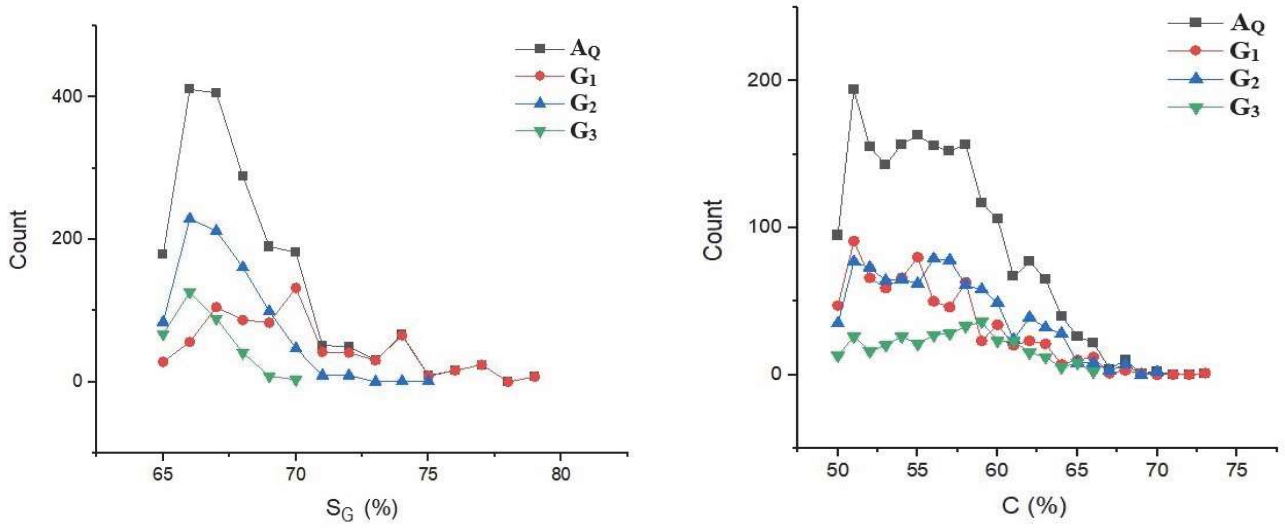

(a) (b)

Figure 5: Count distribution of geometrical parameters of graphite nodules: (a) Sphericity, (b) compactness.

Fig. 6 shows a plot where each nodule of AQ is represented by a grey circle whose coordinates are SG and D. According to the dataset, a nodule concentration zone (NCZ), with ranges of 30-70 μm and 65-70% for D and SG, respectively, was selected. On the other hand, in Fig. 7, the distribution of compactness vs nodule diameter in subpopulation AQ is plotted. Here, another NCZ with ranges of 30-70 μm and 50-63% for D and C, respectively, was selected. It is convenient to evaluate the G1, G2 and G3 nodules within both NCZs to optimize the analysis because the SG and C ranges are well-defined. Therefore, a new subpopulation (AN) is defined. AN adds the nodules concentrated in both zones. Furthermore, 75% of the AQ nodules are included in the AN subpopulation (1476 nodules).

Evaluation of the AN subpopulation

Observing the NCZ of Fig. 6, when SG increases, the small nodule count increases, while the large nodule count decreases. On the other hand, when C increases in the NCZ of Fig. 7, the behaviour is the opposite. The count of the small and large nodules decreases and increases, respectively. These results corroborate the inverse behaviour of G1 and G3 mentioned above. In addition, these results would justify the combined use of both parameters (SG and C) due to their complementary nature. The spatial distribution of the AN subpopulation is shown in Fig. 8, where a nodule uniform distribution and some nodule-clustering zones are observed.

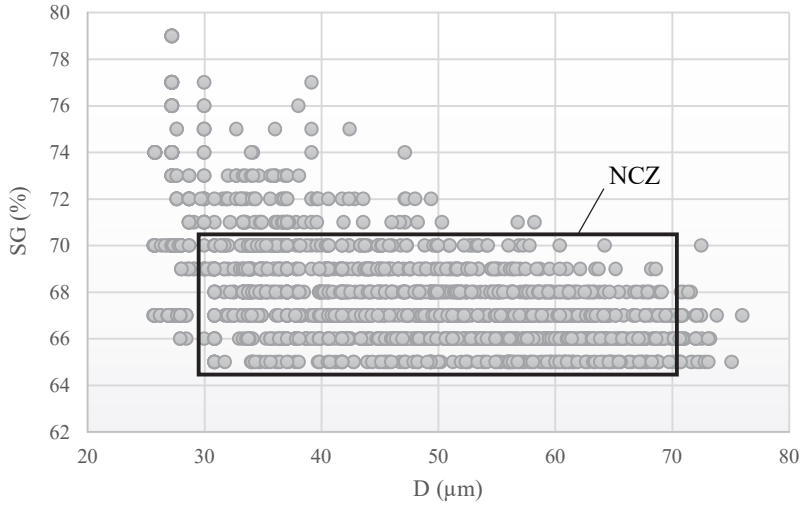

Figure 6: Distribution of sphericity vs nodule diameter in population AQ. NCZ: nodule concentration zone.

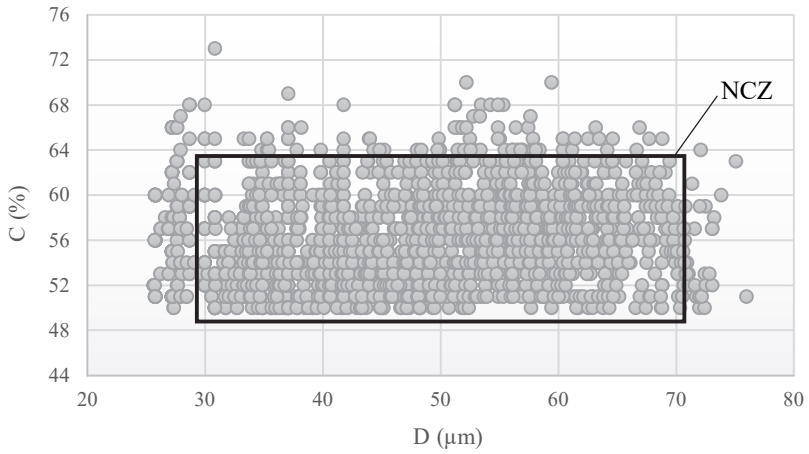

Figure 7: Distribution of compactness vs nodule diameter in population AQ. NCZ: nodule concentration zone.

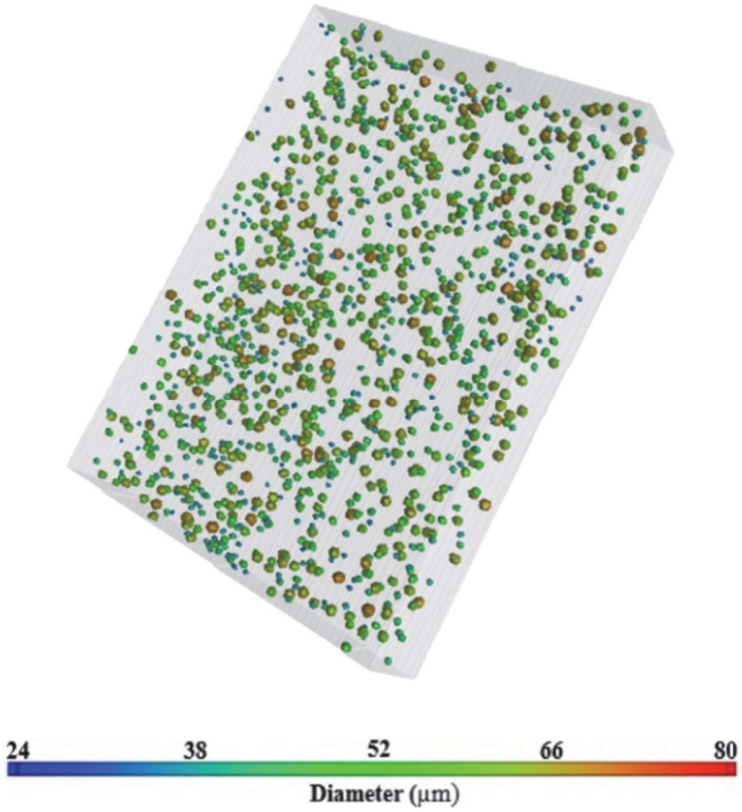

Figure 8: Spatial distribution of the AN subpopulation.

Tab. 3 shows the count for all combinations of SG and C of the AN. The SG and C ranges in the AN subpopulation are 5 and 13%, respectively. Therefore, for the same nodules evaluated, the C values are more diverse, which allow better nodular identification. The higher counts are observed in the 66-67% SG and 51-58% C ranges. These ranges correspond to low and medium values for both parameters. Furthermore, the count is meagre for nodules with high SG and low C and nodules with high C and low SG. It should be noted that, in the work of Díaz et al. [21], the graphite nodule shape is more sensitive to C values than SG values.

S_G (%) \ C (%)	50	51	52	53	54	55	56	57	58	59	60	61	62	63
65	12	26	13	9	11	15	19	8	18	15	4	6	2	2
66	13	34	31	32	37	33	32	35	34	25	23	20	19	15
67	17	23	29	26	25	23	33	28	26	27	21	14	16	16
68	13	23	26	23	27	21	22	21	20	22	17	13	12	10
69	17	12	12	14	12	12	15	16	9	11	8	6	9	10
70	12	7	11	13	9	17	9	9	7	3	5	5	1	3

Table 3: Count for sphericity (SG) and compactness (C) combinations.

Tab. 4 shows the count and the maximum (Cmax) and minimum (Cmin) compactness values associated with each sphericity value. The C range for all SG values is the same (13%), regardless of the count. Each SG value is associated with at least one nodule whose C is maximum and at least one nodule whose C is minimum. It is worth noting that even when the SG value is maximum (70%), the C value can be minimum (50%). Therefore, for each SG value, the nodule quality is associated with the C value.

SG (%)	Count	Cmax (%)	Cmin (%)
65	160	63	50
66	383	63	50
67	324	63	50
68	270	63	50
69	163	63	50
70	111	63	50

Table 4: Count and maximum and minimum compactness for each sphericity value

In the analysis of the different subpopulations, the distinctive combined behaviour of SG and C parameters is highlighted. Therefore, in the morphological evaluation of graphite nodules to define, with accuracy, nodular quality categories, both parameters should be simultaneously evaluated.

Conclusions

This work explores the distances between neighbouring nodules, spatial distributions and clustering tendency, and the combined behaviour of the sphericity and compactness parameters in 1910 high-quality nodules of a ferritic sample using X-ray micro-tomography and digital image processing. The following conclusions can be highlighted:

- The evaluation of the Gap parameter in the AQ population corroborated the high quality of the nodules evaluated. Furthermore, tomographic images show that these nodules are uniformly distributed.
- The exhaustive study of different subpopulations, following a nodular size criterion, revealed the complementary nature of the sphericity and compactness parameters, which define and govern nodular quality.
- From the analysis of the AQ population and following a nodule concentration criterion, a new subpopulation, AN, is defined. AN allowed evaluating the behaviour of different size nodule groups for well-defined ranges of the sphericity and compactness parameters.
- In the AN subpopulation, the study of the link between the nodular size distribution and sphericity and compactness parameters, allowed confirming the complementary nature of these parameters.
- The results in this work not only justify the combined use of the sphericity and compactness parameters to establish nodular quality categories in spheroidal graphite cast iron and other materials, but also provide new perspectives on the nodular morphology study and the distribution of quality nodules in the metallic matrix.

REFERENCES

[1] Angus, H.T. (1976). Cast Iron. Physical and Engineering Properties, Butterworth & Co. (Publishers) Ltd., London.
[2] Minkoff, I. (1983). The physical metallurgy of cast iron, John Wiley and Sons, Hoboken.
[3] Stefanescu, D.M., Alonso, G., Larrañaga, P., De la Fuente E., Suarez, R. (2016). On the crystallization of graphite from liquid iron-carbon-silicon melts. Acta Mater. 107, pp. 102-126. DOI: 10.1016/j.actamat.2016.01.047.
[4] Tewary, U., Paul, D., Mehtani H.K., Bhagavath, S., Alankar, A., Mohapatra, G., et al. (2022). The origin of graphite morphology in cast iron. Acta Mater. 226, 117660. DOI: 10.1016/j.actamat.2022.117660.
[5] Ductile Iron Society (1998). Ductile Iron Data for Design Engineers. Rio Tinto Iron & Titanium, Inc.
[6] Iacoviello, F., Di Cocco, V., Bellini, C. (2019). Fatigue crack propagation and damaging micromechanisms in Ductile Cast Irons, International Journal of Fatigue 124, pp. 48-54, DOI:10.1016/j.ijfatigue.2019.02.030.
[7] Iacoviello, F., Di Cocco, V. (2015). Degenerated graphite nodules influence on fatigue crack paths in a ferritic ductile cast iron. Frattura ed Integrità Strutturale 9, (34), pp. 406–414. DOI: 10.3221/IGF-ESIS.34.45.
[8] Iacoviello, F., Di Cocco, V., Cavallini, M. (2015). Fatigue crack tip damaging micromechanisms in a ferritic-pearlitic ductile cast iron. Frattura ed Integrità Strutturale 9, (33), pp. 111–119. DOI: 10.3221/IGF-ESIS.33.15.
[9] Shiraki, N., Usui, Y., Kanno, T. (2016). Effects of number of graphite nodules on fatigue limit and fracture origins in heavy section spheroidal graphite cast iron. Mater. Trans. 57, pp. 379–384. DOI: 10.2320/matertrans.F-M2015841.
[10] Fernandino, D.O., Boeri R.E. (2016). Fractographic analysis of austempered ductile iron. Fatigue and Fracture of Engineering Materials and Structures 39, (5), pp. 583-598. DOI: 10.1111/ffe.12380.
[11] Fernandino, D.O., Boeri R.E. (2015). Fracture of pearlitic ductile cast iron under different loading conditions. Fatigue and Fracture of Engineering Materials and Structures. 38, (1), pp. 80-90. DOI: 10.1111/ffe.12220.
[12] Di Cocco, V., Iacoviello, F., Rossi, A., Iacoviello, D. (2014). Macro and microscopical approach to the damaging micromechanisms analysis in a ferritic ductile cast iron. Theoretical and Applied Fracture Mechanics 69, pp. 26–33. DOI: 10.1016/j.tafmec.2013.11.003.
[13] Benedetti, M., Fontanari, V., Lusuardi, D. (2019). Effect of graphite morphology on the fatigue and fracture resistance of ferritic ductile cast iron. Engineering Fracture Mechanics 206, (1), pp. 427-441. DOI:10.1016/j.engfracmech.2018.12.019.
[14] Salomonsson, K., Jarfors, A.E. (2018). Three-Dimensional Microstructural Characterization of Cast Iron Alloys for Numerical Analyses. Mater. Sci. Forum 925, pp. 427-435. DOI: 10.4028/MSF.925.427
[15] Andriollo, T., Xu, C., Zhang, Y., et al. (2020). Recent trends in X-ray based characterization of nodular cast iron. Mater. Des. Process. Commun. 3, 1-19. DOI: 10.1002/mdp2.212.
[16] Hanke, R., Fuchs, T., Salamon M., et al. (2016). X-ray microtomography for materials characterization. In: Materials Characterization Using Nondestructive Evaluation (NDE) Methods, Eds.: G. Hübschen, I. Altpeter, R. Tschuncky and H. Herrmann, pp. 45-79.
[17] Louk, A.C., (2014). 3D image reconstruction on X-ray micro-computed tomography. Proceedings Volume 9302. International Conference on Experimental Mechanics. DOI: 10.1117/12.2081193
[18] Lekakh, S.N., Zhang, X., Tucker, W., et al. (2020). Micro-CT Quantitative Evaluation of Graphite Nodules in SGI. Inter. Metalcast. 14, pp. 318–327. DOI: 10.1007/s40962-019-00354-9.
[19] Yin, Y., Tu, Z., Zhou, J., et al. (2017). 3D Quantitative analysis of graphite morphology in ductile cast iron by X-ray microtomography. Metall. Mater. Trans. A 48, pp. 3794–3803. DOI: 10.1007/s11661-017-4130-x.
[20] Chuang, A., Singh, D., Kenesei, P., et al. (2015). 3D quantitative analysis of graphite morphology in high strength cast iron by high-energy X-ray tomography. Scr. Mater.106, pp. 5–8. DOI: 10.1016/j.scriptamat.2015.03.017.
[21] Díaz, F.V., Peralta, M.E., Fernandino, D.O. (2021). Study of sphericity and compactness parameters in spheroidal graphite iron using X-ray micro-computed tomography and image processing. J. Nondestruct. Eval., 40, 11. DOI:10.1007/s10921-020-00738-6.
[22] Muralidhar, C., Subramanian, M.P., Ravi Shankar, V., et al. (2018). Beam hardening effect in computed tomography (CT) – Its relevance and correction in aerospace components. Conference: 2nd International Conference and Exhibition on Advanced Techniques & Practice of Inspection, NDT & Monitoring (INM-2018), New Delhi, 10-11 August.
[23] Ketcham, R.A., Hanna, R.D. (2014). Beam hardening correction for X-ray computed tomography of heterogeneous natural materials. Comput. Geosci. 67, pp. 49-61. DOI: 10.1016/j.cageo.2014.03.003.
[24] Yang, Q., Fullagar,W.K., Myers, G.R., et al. (2020). X-ray attenuation models to account for beam hardening in computed tomography. Appl. Opt. 59, pp. 9126-9136. DOI: 10.1364/AO.402304.

[25] Park, H.S., Chung, Y.E., Seo, J.K. (2015). Computed tomographic beam-hardening artefacts: mathematical characterization and analysis. Phil. Trans. R. Soc. A 373, pp. 20140388. DOI: 10.1098/rsta.2014.0388.
[26] Rodríguez-Sánchez, A., Thompson, A., Körner, L., et al. (2020). Review of the influence of noise in X-ray computed tomography measurement uncertainty. Precis. Eng. 66, pp. 382-391. DOI: 10.1016/j.precisioneng.2020.08.004.
[27] Zhao, Z., Gang, G.J., Siewerdsen, J.H. (2014). Noise, sampling, and the number of projections in cone-beam CT with a flat-panel detector. Med. Phys. 41, 061909. DOI: 10.1118/1.4875688.
[28] Zaky Harun, A., Ab Rashid, R., Ab Razak, K., et al. (2019). Evaluation of contrast-noise ratio (CNR) in contrast enhanced CT images using different sizes of gold nanoparticles. Materials Today: Proceedings 16, (4), pp. 1757-1765. DOI: 10.1016/j.matpr.2019.06.046.
[29] GE Measurement & Control. Available online: https://www.armgate.lv/assets/upload/userfiles/files/phoenix-datos-data-sheet_EN.pdf. Accessed 30 July 2022.
[30] Rueckel, J., Stockmar, M., Pfeiffer, F. (2014). Spatial resolution characterization of an X-ray microCT system. Appl. Radiat. Isot. 94, pp. 230-234. DOI: 10.1016/j.apradiso.2014.08.014.
[31] Volume graphics. Available online: https://www.volumegraphics.com/en/products/vgstudio-max.html. Accessed 30 July 2022.

NOMENCLATURE

CI: Cast Iron
SGI: Spheroidal Grafite cast Iron
μCT: Micro Computerized Tomography
SG: Sphericity
C: Compactness
Ar: Surface of the graphite nodule
Vr: Volume of the graphite nodule
Vs: Volume of the sphere that circumscribes the nodule.
CR: Contrast Resolution
CNR: Contrast to Noise Ratio
ROI: Region of Interest
D: The Diameter of a circumscribed sphere in the graphite nodule
AQ: Graphite Nodule Population defined according to the D, SG and C parameters
G1: Graphite Nodule Subpopulation corresponding to small nodules
G2: Graphite Nodule Subpopulation corresponding to medium nodules
G3: Graphite Nodule Subpopulation corresponding to large nodules
NCZ: Nodular Concentration Zone
AN: Graphite Nodule Subpopulation corresponding to nodules concentrated in the NCZ